Noncritical Quasi-Phase-Matched Second Harmonic Generation in an Annealed Proton-Exchanged $LiNbO_3$ Waveguide

M. L. Bortz, S. J. Field, M. M. Fejer, D. W. Nam, R. G. Waarts, and D. F. Welch

Abstract—**We report the demonstration of dimensional noncritical phase matching, a phase-matched interaction length exceeding 10 mm, and an internal conversion efficiency of 204%/W for second harmonic generation of 976 nm radiation in a periodically poled, annealed proton-exchanged $LiNbO_3$ waveguide. Using models for the linear and nonlinear optical properties of annealed proton-exchanged $LiNbO_3$ waveguides and the observed ferroelectric domain grating, the phase-matching wavelength was predicted to within several nm and the conversion efficiency to within $\approx$20% of the measured values. Optimization of waveguide second harmonic generation devices is discussed.**

I. Introduction

QUASI-PHASE-MATCHED (QPM) second harmonic generation (SHG) in $LiNbO_3$ waveguides is an attractive method for the generation of blue light from infrared diode lasers. Many different techniques have been used to form the ferroelectric domain grating necessary for QPM. Waveguide confinement has been achieved exclusively using the annealed proton exchange (APE) process. While normalized conversion coefficients exceeding 600%/W $\cdot$cm^2 have been reported [1], [2], modeling of the experimentally observed phase-matching wavelengths and normalized conversion efficiencies has not appeared in the literature. The observed phase-matching wavelengths deviate significantly from those predicted from the QPM period and the bulk $LiNbO_3$ refractive indexes. The reported normalized conversion efficiencies, varying from 40 to 700%/W $\cdot$cm^2 [1]–[5], are substantially lower than predicted theoretically. The variations in device performance are due to a combination of factors, including the use of first, second, and third QPM grating orders, different ferroelectric domain grating fabrication processes, and different APE waveguide processing conditions. The discrepancy between the observed and theoretically expected performance is due to inadequate device characterization and an incomplete understanding of the linear and nonlinear optical properties of APE–$LiNbO_3$. The linear optical properties of the waveguide are necessary for calculation of the effective indexes of the guided modes for prediction of the phase-matching wavelength. Both the linear and nonlinear optical properties of the waveguide are necessary for the prediction of the guided wave conversion efficiency. Recently published models for the evolution of the refractive index profile [6] and d_{33} nonlinear coefficient [7] with annealing in APE–$LiNbO_3$ waveguides have yet to be applied to frequency conversion devices.

An additional complication in understanding waveguide frequency conversion devices is the presence of axial phase velocity inhomogeneities. These inhomogeneities can arise from axial variations in the waveguide lithography or processing conditions. Such inhomogeneities reduce the maximum conversion efficiency and distort the ideal sinc^2 tuning curve [8]. Previous work showed that waveguide designs exist that are relatively insensitive to waveguide dimensional fluctuations [9]. This insensitivity arises from eliminating the first-order dependence of the phase velocity mismatch on waveguide dimension, and is termed dimensional noncritical phase-matching in analogy to certain bulk, birefringently phase-matched, nonlinear optical interactions which are insensitive to variations in angle or temperature. Experimentally, noncritically phase-matched interactions should display tuning curves close to ideal, and enhanced interaction lengths over critically phase-matched interactions.

In this paper, we discuss the fabrication, characterization, and analysis of guided wave QPM–SHG devices for $\lambda_\omega \approx 976$ nm fundamental radiation. Phase-matching wavelengths and wavelength tuning curves versus waveguide width are presented that show the evolution towards dimensional noncritical phase matching. Experimental verification of the noncritical phase-matching condition and a phase-matched interaction length exceeding 10 mm are presented. In such a waveguide, an internal conversion efficiency of 204% W was observed, with a corresponding internal normalized conversion efficiency of 185%/W $\cdot$cm^2. The observed phase-matching wavelengths and conversion efficiencies are in good agreement with the expected performance based on recently published models for the linear [6] and nonlinear [7] optical properties of APE–$LiNbO_3$ waveguides. Comparison between observed and expected performance clearly demonstrates the effects that reduce the conversion efficiency of QPM–SHG devices in APE–$LiNbO_3$, and provides guidance towards improvement of the overall device performance.

Manuscript received June 9, 1993; revised May 24, 1994. This work was supported by the Center for Nonlinear Optical Materials, the Joint Services Electronics Program, the Advanced Research Projects Agency, and Crystal Technology, Inc.

M. L. Bortz is with Focused Research, 1275 Reamwood Avenue, Sunnyvale, CA 94089–2256 USA.

S. J. Field and M. M. Fejer are with the E. L. Ginzton Laboratory, Stanford University, Stanford, CA 94305 USA.

D. W Nam, R. G. Waarts, and D. F. Welch are with Spectra Diode Laboratories, Inc., San Jose, CA 95134 USA.

IEEE Log Number 9405197.

II. Experimental

A titanium indiffusion process was used to fabricate ferroelectric domain inversion gratings for quasi-phase-matching [2]. A 50-Å thick Ti film was patterned by wet etching into a grating with 5.00 μm period and 1.0 μm wide lines on the $+z$ face of $LiNbO_3$. Domain inversion was performed by placing the sample on top of congruent $LiNbO_3$ powder in a closed Al_2O_3 crucible and annealing with an approximately linear 2 h ramp to 1100°C for a 4 min soak, after which the furnace was turned off and cooled at approximately 8°C/min. Annealed proton-exchanged waveguides were fabricated after domain inversion by patterning a 2000-Å thick SiO_2 mask with a variety of channel widths, exchanging in pure benzoic acid at 158°C for 90 min to an initial proton exchange depth of 0.22 μm, and annealing for 3 h at 333°C. All process temperatures were measured at the sample position. Waveguide widths quoted in the text are the corresponding mask widths. The sample had multiple waveguides with the same width, and following end face polishing, the device was 10.5 mm long.

The pump laser for SHG measurements was a standing wave titanium–sapphire laser, turned by a Lyot filter and a 3-Å free spectral range etalon, which oscillated in a single longitudinal mode. An isolator was used to prevent feedback into the laser. Laser wavelength was measured to an accuracy of 0.01 Å using a wavemeter. To circumvent complications due to variable input coupling and weak Fabry–Perot resonance effects within the waveguide at the fundamental wavelength (λ_ω), all measurements were performed by monitoring the transmitted fundamental (P_ω) and second harmonic ($P_{2\omega}$) powers separately and recording the ratio $P_{2\omega}/P_\omega^2$, corresponding to the external conversion efficiency. Absolute power measurements are corrected for Fresnel reflections at the exit endface of the waveguide to yield internal conversion efficiencies. Unless noted, all measurements were made with fundamental powers <1 mW to minimize photorefractive or thermal effects in the waveguide. We define the phase-matching wavelength (λ_{pm}) as the wavelength of the observed maximum conversion efficiency, which can differ from the wavelength at which the maximum second harmonic (SH) power is observed due to resonances in the waveguide at λ_ω. The transverse mode structure of the waveguide at the fundamental and the second harmonic ($\lambda_{2\omega}$) wavelengths was monitored using a CCD array, and all the waveguides studied were single transverse mode at the fundamental wavelength.

III. Measurements

Quasi-phase-matched SHG was observed at $\lambda_\omega \approx 1026$ nm with the SH in the transverse TM_{00} mode and at $\lambda_\omega \approx 976$ nm with the SH in the transverse TM_{01} mode (one node in depth), with the exact phase-matching wavelength dependent on waveguide channel width. For comparison, the phase-matching wavelength in bulk $LiNbO_3$ with a 5.00 μm QPM grating is $\lambda_{pm} = 968$ nm [10]. Fig. 1 shows the measured λ_{pm}, with the SH in the transverse TM_{01} mode, as a function of waveguide width (the dashed curve is meant to guide the eye). The scatter in the data is due to two sources: different waveguides of the same nominal width had slightly different phase-matching wavelengths, and the ambient temperature varied by 5°C on different days, represented by the open and closed circles. A maximum in the measured λ_{pm} occurs in waveguides fabricated with mask openings between 5.00 and 5.25 μm. At this maximum, the phase mismatch has no first-order dependence on waveguide width fluctuations, so in the presence of width fluctuations, the maximum phase-matched interaction length should occur in the waveguides with the largest λ_{pm}.

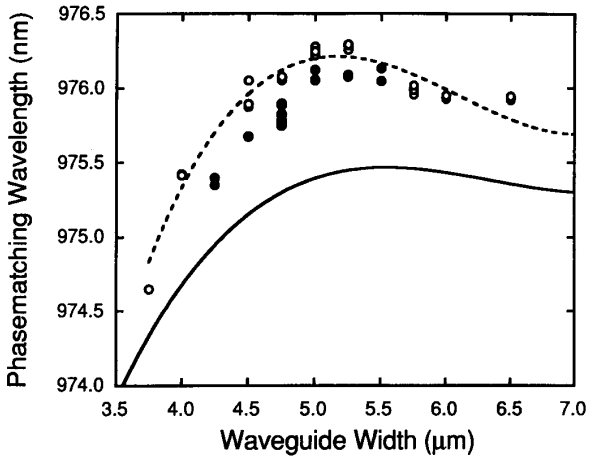

Fig. 1. Measured SHG phase-matching wavelengths versus waveguide width. The open and closed data points were taken at different ambient temperatures. The dashed curve is only meant to guide the eye. The solid curve is the phase-matching wavelengths calculated from the device fabrication conditions using the model described in the text. The maximum in the data represents the dimensional noncritical phase-matching condition, where the phase mismatch has no first-order dependence on waveguide width.

Increased interaction length due to noncritical phase matching was confirmed by measuring the wavelength tuning curves for the TM_{01} mode interaction in waveguides with mask widths of 4.25, 4.50, 5.00, and 5.25 μm, as shown in Fig. 2. The wavelength tuning curves from the waveguides with 4.25 and 4.50 μm widths are far from ideal, with significant conversion efficiency in the wings of the tuning curve and reduced efficiency in the central lobe. As waveguide width increases, the peak conversion increases and the tuning curve narrows. The tuning curve from the 5.00 μm wide waveguide is symmetric and nearly an ideal sinc^2, with a measured wavelength FWHM of 1.1 Å. For wider waveguides, the tuning curves are asymmetric and the peak wavelength remains nearly constant, as shown in Fig. 2(d) for a 5.25 μm wide waveguide. This behavior is consistent with an interpretation of the deviations from the ideal sinc^2 behavior as being due to axial variations in waveguide lithography, which scale with waveguide width.

A useful check of the consistency of these measurements is comparison of the integrated areas under the tuning curves of waveguides of different widths. In a nonlinear optical interaction, the area under the tuning curve is independent of axial phase velocity inhomogeneities [11], which distribute efficiency away from the central lobe into the wings of the tuning curve. The tuning curves shown in Fig. 2 have

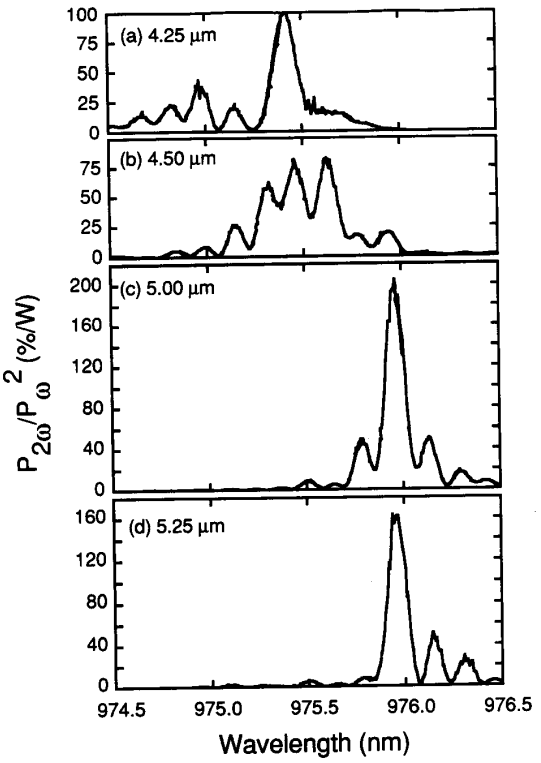

Fig. 2. Measured wavelength tuning curves for waveguides with widths of (a) 4.25 μm, (b) 4.50 μm, (c) 5.00 μm, and (d) 5.25 μm. The ordinate is $P_{2\omega}/P_{\omega}^{2}$, corresponding to power conversion efficiency. Note that only at the dimensional noncritical phase-matching condition does the tuning curve resemble the theoretical sinc^2 shape.

integrated areas that are constant to within 20%, with the area increasing with waveguide width.

The tuning curve for the 5.00 μm wide waveguide indicates that axial inhomogeneities in the grating or the phase velocities are negligible, so this waveguide is ideal for accurate measurements of the normalized conversion efficiency. In this waveguide, the measured internal conversion efficiency was 9.6%/W for SHG into the TM_{00} mode and 204%/W for SHG into the TM_{01} mode. We estimate the accuracy of these measurements to be $\pm 10\%$. Assuming a phase-matched interaction length equal to the 10.5 mm device length, the measured internal normalized conversion efficiencies are $\eta_{TM00} = 8.7\%/\mathrm{W} \cdot \mathrm{cm}^2$ and $\eta_{TM00} = 185\%/\mathrm{W} \cdot \mathrm{cm}^2$. The conversion efficiency of 204%/W is the highest conversion efficiency reported to date in an APE–$LiNbO_3$ waveguide.

IV. Comparison Between Measurements and Calculations

Difficulties in understanding QPM frequency conversion in $LiNbO_3$ waveguides have been exacerbated by inadequate knowledge of the modal properties and the d_{33} nonlinear coefficient of APE– $LiNbO_3$ waveguides. Models for the linear [6] and nonlinear [7] optical properties of APE–$LiNbO_3$ waveguides versus processing conditions were used to predict the phase-matching wavelengths and the normalized conversion efficiencies of the QPM–SHG devices discussed in this work from the QPM grating and waveguide fabrication parameters. Reference [6] contains models for the refractive index profile of APE–$LiNbO_3$ waveguides and material dispersion of APE–$LiNbO_3$ that were used to calculate the two-dimensional refractive index profile of the waveguide [12]. The effective indexes and waveguide mode profiles at λ_ω and $\lambda_{2\omega}$ were then calculated using the effective index method. For a given QPM grating period, the effective indexes determine the wavelength for phase-matching between any set of transverse modes. The normalized conversion efficiencies were calculated using the modes at λ_ω and $\lambda_{2\omega}$, the depth-dependent Fourier component of the QPM grating derived from microscopy of the ferroelectric domain grating, and the variation in the d_{33} coefficient with depth described in [7]. In all cases, the calculations were performed using only the fabrication conditions, with no free parameters. More complete discussion of the linear and nonlinear optical properties of APE–$LiNbO_3$ waveguides will appear elsewhere [13].

The solid line in Fig. 1 shows the phase-matching wavelengths for waveguides formed with a 5.00 μm period QPM grating, calculated using the annealed proton exchange processing parameters described above and mask openings varying from 3.5 to 7 μm. The calculation reproduces the phase-matching wavelength to within several nm, and the calculated maximum at the width of 5.50 μm is in good agreement with the observed maximum between 5.00 and 5.25 μm. For narrower widths, the variation in λ_{pm} with width increases, indicating a large first-order dependence of phase velocity mismatch on waveguide width. The slight offset between the data and the calculation corresponds to an error of about 10^{-4} in the prediction of the effective index dispersion of the APE–$LiNbO_3$ waveguide, which could be due to variations in processing conditions or errors in the model described in [6]. For a 5.00 μm wide waveguide, we calculated $\lambda_{pm} = 1006$ nm and $\lambda_{pm} = 975.4$ nm with the SH in the TM_{00} and TM_{01} modes, respectively, in good agreement with the observed values of $\lambda_{pm} = 1026$ nm and $\lambda_{pm} = 976.1$ nm. The increasing discrepancy at longer wavelengths may be due to increasing error in the effective index method used to calculate the effective indexes as the waveguide approaches cutoff.

Using the model for the APE–$LiNbO_3$ waveguide, we computed the tuning bandwidth for 976 nm frequency doubling with the SH in the TM_{01} mode. Evaluating the waveguide effective indexes N_ω at $\lambda_{pm} = 976$ nm and $N_{2\omega}$ at $\lambda_{2\omega} = 488$ nm yields $dN_\omega/d\lambda_\omega = 7.2 \cdot 10^{-5}\,\mathrm{nm}^{-1}$ and $dN_{2\omega}/d\lambda_{2\omega} = 6.3 \cdot 10^{-4}\,\mathrm{nm}^{-1}$, about 10% greater than the bulk $LiNbO_3$ wavelength derivatives. Using these values, we compute a wavelength FWHM tuning bandwidth of 12.6 Å · mm for $\lambda_{pm} = 976$ nm. From the tuning curve shown in Fig. 2(c), the observed FWHM bandwidth indicates an interaction length of 11.4 mm, in reasonable agreement with the actual 10.5 mm device length.

We also compared the experimental normalized conversion efficiencies to the theoretical values. With the direction of propagation along the x axis over a phase-matched interaction length l, the ideal, lossless, internal normalized conversion

efficiency η_0, defined by $P_{2\omega} = \eta_0 P_\omega^2 l^2$, is given by

$$\eta_0 = \frac{8\pi^2 d_{\text{eff}}^2}{N_\omega^2 N_{2\omega} c\varepsilon_0 \lambda_\omega^2} \left| \int_{-\infty}^{+\infty} dy \int_0^{+\infty} dz G_m(z)\, \bar{d}(z) \cdot E_{2\omega}(y,z) E_\omega^2(y,z) \right|^2. \quad (1)$$

In this expression, $d_{\text{eff}} = 2 \cdot d_{33}/\pi m, m$ is the order of the quasi-phase matching, $\bar{d}(z) = d_{33}^{\text{APE}}(z)/d_{33}^{LN}$ is the d_{33} nonlinear coefficient in the APE–$LiNbO_3$ waveguide normalized to the bulk $LiNbO_3$ value, and E_ω and $E_{2\omega}$ are the optical modes normalized to carry unity power. P_ω is the fundamental power coupled into the waveguide. We have explicitly included the depth dependence of the d_{33} nonlinear coefficient within the overlap integral. The term $G_m(z)$ is the depth-dependent Fourier coefficient of the QPM grating defined as

$$G_m(z) = \frac{m\pi}{2} \left(\frac{1}{\Lambda_g} \int_0^{\Lambda g} g(x,z) e^{-i(2m\pi/\Lambda_g)x}\, dx \right) \quad (2)$$

where Λ_g is the QPM grating period and $g(x,z)$ is the function that describes the spatial variation of the ferroelectric domain grating, taking a value $+1(-1)$ in $+z(-z)$-oriented domains. For the first-order QPM ($m = 1$) devices described in this work, $G(z) = \sin\{\pi\xi(z)\}$, where $\xi(z)$ is the depth-dependent duty cycle of the grating which takes a value of 1/2 for ideal first-order QPM. In subsequent calculations, we take 34.5 pm/V as the value of the d_{33} nonlinear coefficient in bulk $LiNbO_3$, and use the measurements of [7] for the depth dependence of $\bar{d}(z)$, the nonlinear coefficient in the APE–$LiNbO_3$ waveguide.

Assuming the modes are separable (i.e., $E(y,z) = E_y(y)E_z(z)$), the above expression for η_0 simplifies to

$$\eta_0 = \frac{8\pi^2 d_{\text{eff}}^2}{N_\omega^2 N_{2\omega} c\varepsilon_0 \lambda_\omega^2} I_z^2 I_y^2$$

with

$$I_z = \int_0^\infty G_m(z)\bar{d}(z) E_{2\omega}(z) E_\omega^2(z)\, dz$$
$$I_y = \int_{-\infty}^\infty E_{2\omega}(y) E_\omega^2(y)\, dy. \quad (3)$$

In the limit of negligible loss and ignoring the Fabry–Perot resonances within the waveguide (these effects and their influence on measurement of the normalized conversion efficiency are discussed in the Appendix), the experimentally observed normalized conversion efficiency and the ideal, theoretical normalized conversion efficiency defined in (1)–(3) are equivalent quantities suitable for comparison.

Fig. 3(a) shows a schematic of the periodic QPM ferroelectric domain grating used in this work, revealed after endface polishing by etching in pure HF for 5 min. The grating angle θ is 24° and the buried grating depth a is 1.1 μm. Fig. 3(b) and (c) show the factors entering into the integrand of I_z for phase-matching into the TM_{00} and TM_{01} SH modes for the 5.00 μm wide noncritically phase-matched waveguide previously discussed. The integrands of I_y are not shown for brevity since they depend only on the optical modes. The dashed curves are the square of the modal field at λ_ω and the modal field at $\lambda_{2\omega}$ calculated using the results of [6], the solid curve is the first Fourier component of the observed grating, and the dotted curve is the depth dependence of $\bar{d}(z)$ in the APE–$LiNbO_3$ waveguide. The integrand of $I_z, G(z)\bar{d}(z)E_{2\omega}(z)E_\omega^2(z)$, is shown as the hatched portion in Fig. 3(b) and (c). As discussed in [7], the d_{33} coefficient of an APE–$LiNbO_3$ waveguide is reduced within the initial proton exchange depth, but retains the bulk $LiNbO_3$ value at depths greater than the initial proton exchange depth throughout the annealing process. For this device, the initial proton exchange depth is 0.22 μm, while the grating is buried by 1.1 μm. Thus, the grating Fourier component is zero for depths less than 1.1 μm, and in this device, the conversion efficiency is unaffected by the degradation of the d_{33} coefficient due to the APE process. The ideal modal overlap assuming a perfect rectangular grating (i.e., $G(z) = 1$ and $\bar{d}(z) = 1$) yields the internal normalized conversion efficiency of $\eta_{TM00} = 404\%/\text{W} \cdot \text{cm}^2$ and $\eta_{TM01} = 675\%/\text{W} \cdot \text{cm}^2$. However, including the effect of the grating, we compute normalized conversion efficiencies of $\eta_{TM00} = 13.2\%/\text{W} \cdot \text{cm}^2$ and $\eta_{TM01} = 215\%/\text{W} \cdot \text{cm}^2$, in very good agreement with the observed values of $\eta_{TM00} = 8.7\%\,\text{W} \cdot \text{cm}^2$ and $\eta_{TM01} = 185\%\,\text{W} \cdot \text{cm}^2$. The grating shape and position cause η_{TM01} to greatly exceed η_{TM00}; note that the cancellation of the modal overlap where the TM_{01} SH mode is negative is eliminated since the grating Fourier coefficient is zero at these depths. While the agreement between the observed and calculated results is encouraging, direct comparison between the absolute experimental and theoretical conversion efficiencies is complicated by several factors described in the Appendix. Another measure of the accuracy of the calculations shown in Fig. 3(b) and (c) is the ratio of the conversion efficiencies for phase-matching into the different transverse modes; such a ratio serves to reject absolute measurement error, uncertainties in the d_{33} coefficient of bulk $LiNbO_3$, etc. The observed value of $\eta_{TM01}/\eta_{TM00} = 21.3$ compares well with the calculated value $\eta_{TM01}/\eta_{TM00} = 16.3$.

It was noted above that the wavelength tuning curves shown in Fig. 2 for waveguides of different widths have integrated areas that are constant to within about 20%, with the area increasing with waveguide width. In a bulk nonlinear optical interaction, the area under the tuning curve is independent of axial phase velocity inhomogeneities. However, in a waveguide, changing the nominal width leads to changes in the transverse overlap integral defined by (1)–(3) in addition to changes in the sensitivity to phase velocity inhomogeneities. Calculations similar to the one shown in Fig. 3(c) indicate a reduction in the integrated areas of $\approx 5\%$ between the 4.25 and 5.25 μm wide waveguide due to the transverse overlap. The remaining variation in the areas is probably due to increasing loss with decreasing waveguide width, expected if the dominant loss mechanism is sidewall scatter.

Fig. 3 indicates that the η_{TM00} conversion efficiency may be significantly improved by reducing the buried depth a of the ferroelectric domain grating. While changing the shape of the grating may prove difficult with the Ti-induced domain inversion process, a may be reduced by either lowering the

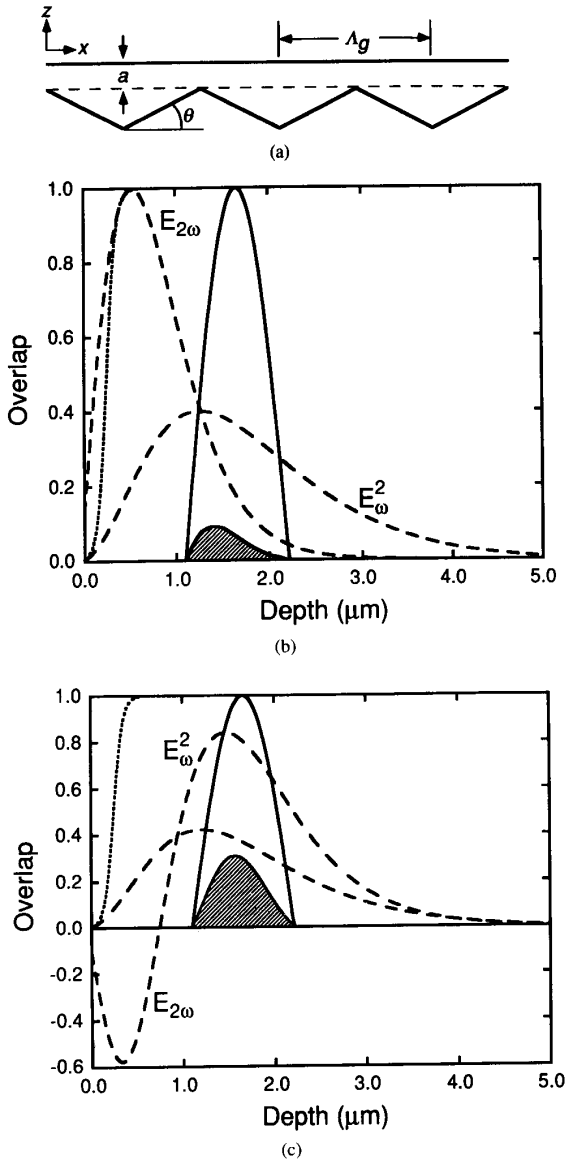

Fig. 3. Depth overlap integral calculations for the 5.00 μm wide waveguide. (a) shows a schematic diagram spatial variation of the ferroelectric domain grating, and hence $g(x,z)$: $\Lambda = 5.0\,\mu\text{m}, \theta = 24°$, and $a = 1.1\,\mu$m. In (b) and (c), the dashed curves are E^2_ω and $E_{2\omega}$, the solid curve is the grating function $G(z)$, the dotted curve is the normalized d_{33} coefficient in the waveguide, and the hatched area is the integrand of I_z for (b) the second harmonic in the TM_{00} mode and (c) the second harmonic in the TM_{01} mode.

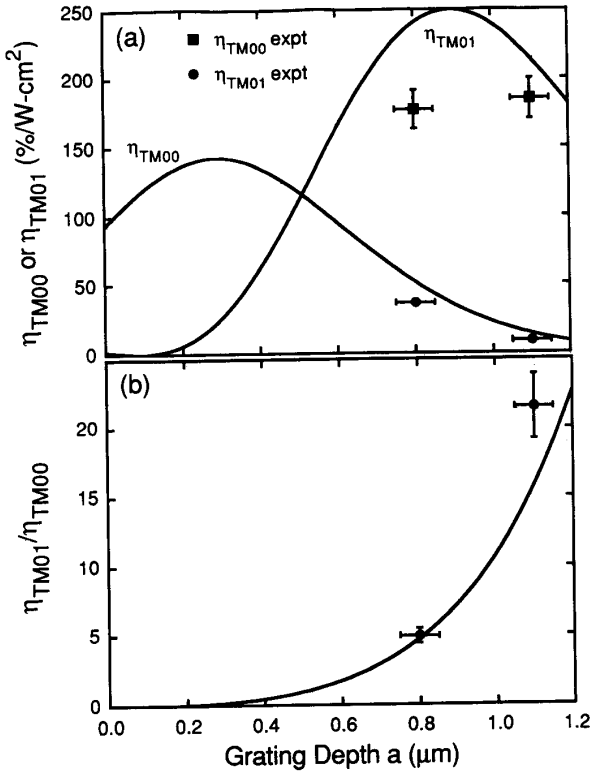

Fig. 4. (a) Comparison between experimental and theoretically predicted external normalized conversion efficiency for phase matching into the TM_{00} and TM_{01} SH mode versus grating depth a. The waveguide fabrication conditions are described in the text. The circles are measured conversion efficiencies for devices with different grating fabrication conditions. (b) Comparison between experimental and theoretically predicted ratio η_{TM01}/η_{TM00} versus grating depth a.

soak temperature of shortening the soak times of the Ti diffusion. Another domain inversion grating was fabricated with a soak temperature of 1090°C rather than 1100°C, with all other diffusion parameters the same as previously described. This domain grating had a shape nearly identical to that shown in Fig. 3(a) with a buried depth $a = 0.8\,\mu$m. APE waveguides were fabricated as previously discussed. In the 5.00 μm wide waveguide, a near ideal tuning curve was observed with a FWHM of 3.0 Å, corresponding to an interaction length of 4.2 mm, in good agreement with the 4.4 mm sample length. The measured normalized conversion efficiencies in this waveguide were $\eta_{TM00} = 36$ and $\eta_{TM01} = 177\%/\text{W} \cdot \text{cm}^2$ for SHG into the TM_{00} and TM_{01} SH modes, respectively. Fig. 4(a) shows the measured and calculated normalized conversion efficiencies in the 5.00 μm wide waveguide versus a. Fig. 4(b) shows the measured and calculated ratio η_{TM01}/η_{TM00}. Modifying the grating position increases η_{TM00} and decreases the ratio η_{TM01}/η_{TM00} by a factor of 4, in good agreement with the theoretical results. The agreement between experiment and theory when the actual domain grating is used in the calculation substantially confirms the previously presented models for the linear and nonlinear optical properties of APE–$LiNbO_3$. In this sample, we measured a maximum blue output power of 5.1 mW with 163 mW of fundamental radiation exciting the waveguide. This corresponds to a conversion efficiency about 1/2 that measured at low input powers.

Fig. 4 indicates that the Ti-diffusion process for domain inversion and an adequate reduction of the grating depth should result in conversion efficiencies approaching 150%/W $\cdot \text{cm}^2$ for SHG into the TM_{00} mode. For phase matching 976 nm radiation, this requires a grating period shorter than

the 5.00 μm period discussed above. Preliminary experiments for SHG of 976 nm radiation with a 4.5 μm ferroelectric domain grating and a grating depth of $a = 0.3\,\mu$m show normalized conversion efficiencies 140%/W $\cdot$cm^2; these devices will be discussed along with high-power effects in a future publication. Further efficiency gains may be achieved by a deeper, depth-independent domain grating and by tighter waveguide confinement, as is clear from the low modal overlap and extended fundamental mode shown in Fig. 3(b) and (c). Normalized conversion efficiencies of 150%/W $\cdot$cm^2 in a TM_{00} mode and interaction lengths exceeding 10 mm should prove sufficient for many device applications that require 488 nm radiation.

V. Conclusion

We have demonstrated noncritical phase matching and interaction lengths exceeding 10 mm in a quasi-phase-matched annealed proton-exchanged $LiNbO_3$ waveguide. An internal conversion efficiency of 204%/W over a 10 mm interaction length was achieved using the Ti-indiffusion process for ferroelectric domain inversion and tailoring the APE–$LiNbO_3$ waveguide for dimensional noncritical phase matching. We have accurately modeled the phase-matching wavelengths and conversion efficiencies of these devices using recently available models for the linear and nonlinear optical properties of APE–$LiNbO_3$. The degradation of the d_{33} coefficient does not affect these devices, but may play a role in limiting the conversion efficiencies of other guided wave SHG devices, especially those with tighter modal confinement than was used here. Dimensional noncritical phase-matching and the accompanying reduction in axial phase velocity inhomogeneities allow a detailed examination of device performance, and are essential for understanding and improving guided wave QPM frequency conversion devices.

Appendix

Measurement of normalized conversion efficiencies in waveguide frequency conversion devices is complicated by a variety of factors, including grating and/or waveguide inhomogeneities, propagation loss in the waveguide, resonance effects within the waveguide, the mode structure of the pump laser, and the magnitude of the relevant material parameters such as the bulk nonlinear coefficient. Accurate measurement and analysis of the normalized conversion efficiency is important for device engineering and optimization. This Appendix treats some of these effects.

Grating and waveguide inhomogeneities can have a large effect on conversion efficiency. Some types of inhomogeneities do not modify the tuning curves, but reduce the device conversion efficiency [8]. In general, these inhomogeneities locally reduce the magnitude of the pertinent grating Fourier component. As an example of this type of inhomogeneity, we consider duty cycle variations in the ferroelectric domain grating, observed as a slightly varying shape of the Ti-diffused domain grating shown in Fig. 3(a) and recently in electric field periodically poled $LiNbO_3$ [1]. In the case of random duty cycle errors with a fixed period defined by lithography, the expectation value of the conversion efficiency $\langle\eta\rangle$ normalized to η_0, the ideal, internal normalized conversion efficiency calculated from (1)–(3), is given by [14]

$$\frac{\langle\eta\rangle}{\eta_0} \cong \exp\left[-(\sqrt{2}\pi\sigma/\Lambda_g)^2\right] \tag{A1}$$

where Λ_g is the QPM grating period and σ is the rms error in the duty cycle, assumed to be normally distributed. rms errors as large as 1/6 of Λ_g reduce the conversion efficiency by only 50%. The duty cycle effect is probably smaller than other measurement and analysis errors in this work, but may be relevant for the devices described in [1].

The annealed proton-exchanged waveguide fabrication process can yield low-loss waveguides. However, even loss values of $\approx$1–2 dB/cm can have a significant effect of the nonlinear frequency conversion process. In the presence of phase velocity mismatch and propagation loss, the conversion efficiency normalized to η_0 is given by [15]

$$\frac{\eta(\Delta k, \alpha_\omega, \alpha_{2\omega})}{\eta_0} = 2e^{-[(\alpha_\omega+\alpha_{2\omega}/2)l]} \cdot \left(\frac{\cosh(\Delta\alpha l) - \cos(\Delta k l)}{(\Delta\alpha l)^2 - (\Delta k l)^2}\right) \tag{A2}$$

where α_ω and $\alpha_{2\omega}$ are the exponential power loss coefficients at λ_ω and $\lambda_{2\omega}$ and $\Delta\alpha = \alpha_{2\omega}/2 - \alpha_\omega$. The phase-matching bandwidth is a function of the combined loss parameter $\Delta\alpha$. Fig. 5 shows the FWHM bandwidth normalized to the lossless case versus $\Delta\alpha l$. There is a negligible effect on the bandwidth and little distortion of the ideal sinc^2 tuning curve for $\Delta\alpha l < 2$, a condition obeyed by typical APE waveguides. However, this is not the case for the phase-matched conversion efficiency, given by

$$\frac{\eta(\Delta k = 0, \alpha_\omega, \alpha_{2\omega})}{\eta_0} = e^{-2\alpha_\omega l}\left(\frac{1 - e^{-\Delta\alpha l}}{\Delta\alpha l}\right)^2. \tag{A3}$$

Fig. 6 shows the conversion efficiency normalized to η_0 versus $\alpha_\omega l$ for different values of $\alpha_{2\omega}/\alpha_\omega$. As an example, a 1 dB single-pass loss at both λ_ω and $\lambda_{2\omega}$ leads to $a \approx 25\%$ reduction in the peak conversion efficiency.

The above expressions for conversion efficiency in the presence of loss are referenced to the fundamental power coupled into the waveguide, while the experimental conversion efficiencies quoted in this work and in most of the literature are referenced to the fundamental power after propagation over the length of the waveguide (there is a further distinction between the internal and external conversion efficiencies, with the former correcting the measured powers for Fresnel reflections at the waveguide endface). In the presence of propagation loss, the fundamental power coupled into the waveguide and the fundamental power remaining in the waveguide after propagating over a length l are related by $P_\omega(l) = P_\omega(0)e^{-\alpha_\omega l}$. The ratio of the phase-matched conversion efficiency, referenced to the fundamental power after propagation over a length l, to η_0 is given by

$$\frac{\eta(\Delta k = 0, \Delta\alpha)}{\eta_0} = \left(\frac{1 - e^{-\Delta\alpha l}}{\Delta\alpha l}\right)^2. \tag{A4}$$

$$\frac{\eta}{\eta_0} = \frac{\operatorname{sinc}^2\left(\beta\Delta\lambda_\omega(N_{2\omega}(\lambda_{2\omega}) - N_\omega(\lambda_\omega) - 1/\Lambda_g)\right)}{[(1-R_\omega)^2 + 4R_\omega \sin^2(\beta N_\omega(\lambda_\omega))]^2[(1-R_{2\omega})^2 + 4R_{2\omega}\sin^2(2\beta N_{2\omega}(\lambda_{2\omega}))]} \tag{A5}$$

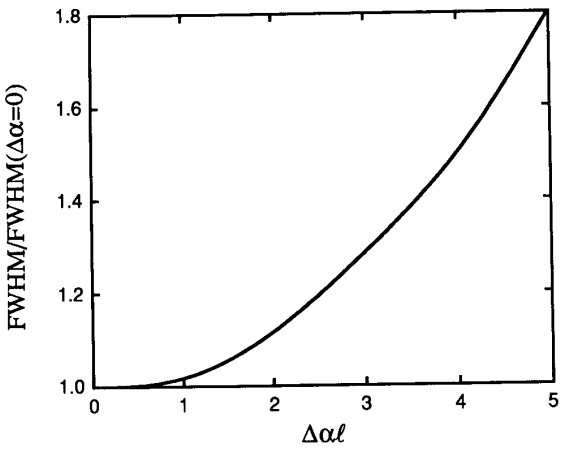

Fig. 5. Increase in FWHM bandwidth versus combined loss parameter $\Delta\alpha = \alpha_\omega - \alpha_{2\omega}/2$. Annealed proton-exchanged $LiNbO_3$ waveguides can be fabricated with low enough losses that the bandwidth increase is negligible.

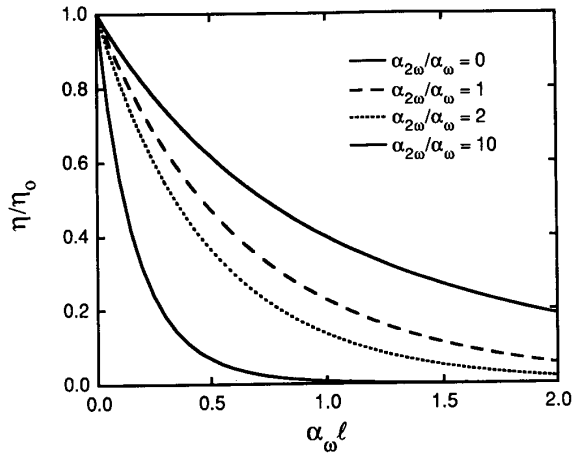

Fig. 6. Reduction in phase-matched conversion efficiency, normalized to the lossless case, versus $\alpha_\omega \ell$ for different values of $\alpha_{2\omega}/\alpha_\omega$. Even high-quality, low-loss APE–$LiNbO_3$ waveguides will exhibit a reduced conversion efficiency due to loss.

This expression gives the surprising result that the error between η_0 and the measured conversion efficiency when normalized to the transmitted fundamental power depends on the combined loss parameter $\Delta\alpha$ rather than α_ω and $\alpha_{2\omega}$ considered separately. $\eta/\eta_0 = 1$ when $\alpha_{2\omega} = 2 \cdot \alpha_\omega$ and decreases with increasing loss at the second harmonic. Since $\Delta\alpha$ depends on the exponential loss coefficients, even losses of 3 dB at the SH and 1 dB at the fundamental only result in $\approx 10\%$ error when comparing η to the ideal expression η_0. The insensitivity of η/η_0 to loss arises from the competing effects of loss on the SHG interaction; loss reduces the driving nonlinear polarization along the waveguide, resulting in less SH output, but loss also reduces the throughput of the fundamental, increasing the apparent conversion efficiency when referenced to the transmitted power. When $\Delta\alpha$ is small, the effects essentially offset each other, and reasonably accurate measurements of η_0 can be obtained by using the transmitted fundamental power to determined the conversion efficiency.

If a waveguide device has polished endfaces with the surface normal nearly aligned to the waveguide propagation direction, the waveguide acts as a weak resonator at λ_ω and $\lambda_{2\omega}$. The transmitted and circulating power at the fundamental wavelength oscillate with waveguide temperature or incident wavelength due to the Fabry–Perot resonance. There is a similar effect at $\lambda_{2\omega}$. In the presence of resonance, the ratio of the conversion efficiency, referenced to the fundamental power coupled into the waveguide, to η_0 is given by (A5), shown at the top of the page, where R_ω and $R_{2\omega}$ are the waveguide endface power reflectivities and $\beta = 2\pi l/\lambda_\omega$. A tuning curve of $P_{2\omega}$ versus Δk will have fringes due to resonance at λ_ω and $\lambda_{2\omega}$. The sinc^2 phase-matching envelope is modulated by fringes that, depending on device length and λ_ω, can have a periodicity ranging from much less to much greater than the FWHM phase-matching bandwidth. By recording the transmitted powers at λ_ω and $\lambda_{2\omega}$ and referencing the conversion efficiency to the transmitted fundamental power, the fringes due to the fundamental wavelength resonance may be removed. Fringes due to the second harmonic resonance remain, but are usually less of a problem due to increased loss at shorter wavelengths. Accurate measurements of the conversion efficiency and phase-matching wavelengths are facilitated by waveguide endface angle polishing and antireflection coating to reduce the resonance effects.

The expressions for the conversion efficiency used in this work assume a single axial mode pump source. Multiple axial pump modes can mix in the nonlinear frequency conversion interaction with a complicated effect on conversion efficiency. In the case of a pump source with multiple axial modes with uncorrelated phases and a total bandwidth significantly less than the phase-matching bandwidth, the ratio of the conversion efficiency to η_0 is given by [16]

$$\frac{\eta_{\text{multimode}}}{\eta_0} = \left(2 - \frac{1}{N}\right) \tag{A6}$$

where N is the total number of axial modes. As an example, a standing wave Ti : sapphire laser with a 200 MHz free spectral range may have 50 modes oscillating in a 10 GHz bandwidth, considerably less than a typical 1-Å SHG device bandwidth. In this case, one may expect an enhancement of ≈ 2 over the single mode case. However, in a typical laser diode, the output power may be evenly distributed among four axial modes with

a mode spacing of ≈ 5 Å, far greater than the SHG phase-matching bandwidth. The maximum conversion efficiency in this case would be reduced by a factor of 16 compared to the ideal single-mode case. Thus, a single SHG device can exhibit conversion efficiencies that easily vary by over an order of magnitude due to the spectral content of typical laboratory pump sources.

Finally, analysis of quasi-phase-matched $LiNbO_3$ frequency conversion devices requires a value for the d_{33} nonlinear coefficient of bulk $LiNbO_3$. However, values in the literature range from 27 [17] to 34.5 pm/V [18], resulting in analysis errors of $\approx 50\%$. Recent measurements of 23.7 pm/V [19] reemphasize the continuing need for accurate measurements of bulk nonlinear coefficients.

ACKNOWLEDGMENT

The authors are grateful to R. Sadowski and M. Digonnet for the loan of equipment used in testing the devices.

REFERENCES

[1] M. Yamada, N. Nada, M. Saitoh, and K. Watanabe, "First order quasi-phasematched $LiNbO_3$ waveguide periodically poled by applying an external field for efficient blue second harmonic generation," *Appl. Phys. Lett.*, vol. 62, pp. 435–436, 1993.

[2] M. Fujimura, K. Kintaka, T. Suhara, and H. Nishihara, "Blue light generation in a $LiNbO_3$ waveguide second harmonic generation device with first order domain inverted grating formed by EB scanning," *Electron. Lett.*, vol. 28, pp. 1868–1869, 1992.

[3] E. J. Lim, M. M. Fejer, R. L. Byer, and W. J. Kozlovsky, "Blue light generation by frequency doubling in a periodically poled $LiNbO_3$ channel waveguide," *Electron Lett.*, vol. 25, pp. 731–732, 1989.

[4] F. Armani, D. Delacourt, E. Lallier, M. Papuchon, Q. He, M. De Micheli, and D. B. Ostrowski, "First order quasi-phasematching in $LiNbO_3$," *Electron. Lett.*, vol. 28, pp. 139–140, 1992.

[5] X. Cao, B. Rose, R. V. Ramaswamy, and R. Srivastava, "Efficient direct diode laser frequency doubling in quasi-phasematched $LiNbO_3$ waveguide," *Opt. Lett.*, vol. 17, pp. 795–797, 1992.

[6] M. L. Bortz and M. M. Fejer, "Annealed proton exchanged $LiNbO_3$ waveguides," *Opt. Lett.*, vol. 6, pp. 1844–1846, 1991.

[7] M. L. Bortz, L. A. Eyres, and M. M. Fejer, "Depth profiling of the d_{33} nonlinear coefficient in annealed proton exchanged $LiNbO_3$ waveguides," *Appl. Phys. Lett.*, vol. 61, pp. 2012–2014, 1993.

[8] S. Helmfrid, G. Arvidsson, and J. Webjorn, "Influence of various imperfections on the conversion efficiency of second harmonic generation in quasi-phasematched lithium niobate waveguides," *J. Opt. Soc. Amer. B*, vol. 10, pp. 222–229, 1992.

[9] E. J. Lim, S. Matsumoto, and M. M. Fejer, "Noncritical phasematching for guide wave frequency conversion," *Appl. Phys. Lett.*, vol. 57, pp. 2294–2296, 1990.

[10] M. Lawrence and G. Edwards, "A temperature dependent dispersion equation for congruently grown lithium niobate," *Opt. Quantum Electron.*, vol. 16, pp. 373–374, 1984.

[11] F. R. Nash, G. D. Boyd, M. Sargent, III, and P. M. Bridenbaugh, "Effect of optical inhomogeneities on phasematching in nonlinear crystals," *J. Appl. Phys.*, vol. 41, pp. 2564–2576, 1970.

[12] An implicit finite difference algorithm was used to solve for the refractive index distribution and the effective index method was used to solve for the electric field modes.

[13] M. L. Bortz, M. M. Fejer, and K. Kissa, to be submitted to *IEEE J. Quantum Electron.*

[14] M. M. Fejer, G. A. Magel, D. H. Jundt, and R. L. Byer, "Quasi-phasematched second harmonic generation: Tuning and tolerances," *IEEE J. Quantum Electron.*, vol. 28, pp. 2631–2654, 1992.

[15] J. Zyss and D. S. Chemla, in *Nonlinear Optical Properties of Organic Molecules and Crystals*, D. S. Chemla and J. Zyss, Eds. Orlando, FL: Academic, 1987, ch. 1, pp. 42–43.

[16] J. Ducuing and N. Bloembergen, "Statistical fluctuations in nonlinear optical processes," *Phys. Rev.*, vol. 133, pp. A1493–A1502, 1964.

[17] R. C. Miller, W. A. Nordland, and P. M. Bridenbaugh, "Dependence of second harmonic generation coefficients of $LiNbO_3$ on melt composition," *J. Appl. Phys.*, vol. 42, pp. 4145–4147, 1971.

[18] M. M. Choy and R. L. Byer, "Accurate second-order susceptibility measurements of visible and infrared nonlinear crystals," *Phys. Rev. B*, vol. 14, pp. 1693–1706, 1976.

[19] T. Kondo, I. Shoji, K. Yashiki, and R. Ito, "Absolute nonlinear optical coefficient measurements using a laser diode," in *Quantum Electronics and Laser Science Conf. 1992 OSA Tech. Dig. Ser. Vol. 13,* Opt. Soc. Amer., Washington, DC, 1992, pp. 242–244.

M. L. Bortz, photograph and biography unavailable at the time of publication.

S. J. Field, photograph and biography unavailable at the time of publication.

M. M. Fejer, photograph and biography unavailable at the time of publication.

D. W. Nam, photograph and biography unavailable at the time of publication.

R. G. Waarts, photograph and biography unavailable at the time of publication.

D. F. Welch, photograph and biography unavailable at the time of publication.